Synthetic Metals, 3 (1981) 89 - 98

LOW FREQUENCY PLASMON SPECTRA IN STAGE I AND STAGE II $FeCl_3$ INTERCALATED GRAPHITE

EUGENE J. MELE and JOHN J. RITSKO
Xerox Webster Research Center, Webster, New York 14580 (U.S.A.)
(Received May 19, 1980)

Summary

Theoretical analyses of plasmon lineshapes and dispersion in model stage I and stage II graphite intercalation compounds (GIC's), with application to $FeCl_3$ intercalated graphites are presented. From a general analytic model of the longitudinal dielectric response functions we discuss the electronic properties of graphite intercalation compounds which are effectively probed in inelastic electron scattering spectra below 3 eV. Band structure and local field effects are then explicitly included in numerical calculations of energy loss spectra in these compounds. We note that band structure effects are very significant in determining plasmon dispersion and damping in these compounds, and find that a model band structure with band parameters extracted from previous studies of pristine graphite provides a good description of the observed spectra.

1. Introduction

Excitation spectra of both valence [1, 2] and core electrons [3, 4] in graphite intercalation compounds are currently being probed with inelastic electron scattering spectroscopy. The measurement of valence excitations by this technique is proving to be especially fruitful, as it allows a mapping of the momentum transfer (q) dependence of a characteristic low frequency plasmon in these compounds, which is generally observed as a plasma edge in optical ($q = 0$) measurements. This excitation is due to a plasma oscillation of the intercalation induced charge in the graphite layers, and measurement of its evolution with q provides direct information about the dispersion of both intraband electronic excitations and interband electronic transitions in these systems [1, 5]. In this paper we briefly outline our analyses of inelastic electron scattering spectra in stages I and II $FeCl_3$ intercalated graphite and examine the characteristic low frequency electronic excitations in these compounds.

2. General considerations

The electronic properties of GIC's which are probed in these experiments are illustrated in the following simple analytic model. Consider a gas of electrons described by a lattice of stacked charge sheets, with repeat length d. In each sheet the electrons obey a dispersion relation $E(k) = \beta|k|$ where k is directed in the basal plane. For $|q| \ll |k_F|$ we may then approximate the longitudinal dielectric response function for this system:

$$\epsilon(q, \omega) \approx \epsilon_\infty + f(q, d) \frac{e^2}{|q|^2} \frac{G(q) < |q \cdot \nabla_q E|>}{\langle |q \cdot \nabla_q E| \rangle^2 - \omega^2} \tag{1}$$

where in the limit $q/k_F \ll 1$

$$G(q) = 6qk_F/(2\pi)^2. \tag{2}$$

In the above k_F is the Fermi momentum of the two dimensional electron gas, ϵ_∞ is a background dielectric constant and $\langle\ \rangle$ denote an average over all azimuthal angles. In this approximate expression we have replaced the intraband continuum by an average oscillator at $\omega = \langle |q \cdot \nabla_q E| \rangle$ with degeneracy $G(q)$. The $f(q, d)$ is a function which is asymptotic to $4\pi/d$ from above in the limit $qd \to 0$. The deviation of f from this value for larger qd, results from local field corrections which we discuss in more detail in Section 4. For now, we note that these corrections are correctly included in eqn. (1) only near the plasma frequency. The zeroes of eqn. (1) then define a plasmon dispersion relation

$$\omega^2{}_p = (\tilde{\beta} q)^2 + \Omega_0{}^2 \tag{3}$$

where

$$\Omega_0{}^2 = 6e^2(k_F\beta)/(\pi d\epsilon_\infty) \tag{4a}$$

and

$$\tilde{\beta} = 2\beta/\pi. \tag{4b}$$

Hence

$$\omega_p(q) = \Omega_0 + \tilde{\beta}^2 q^2/(2\Omega_0) \tag{5}$$

for small q. Equations (4a) and (5) illustrate the principal results. Ω_0 denotes the plasmon measured in an optical experiment. From eqn. (4) we see that Ω_0 scales as $(k_F\beta)^{1/2}$, *i.e.*, as the square root of the shift of the Fermi energy in a GIC. Further knowledge of β, obtainable, for instance, from a band calculation, may then be used to determine k_F or equivalently the two dimensional charge density [6]. Note, however, that given an accurate value of β the measured plasma frequency scales only as the fourth root of the two dimensional charge density. From eqn. (5) we expect the dispersion of the plasmon to be quadratic at small q. This power law with which the plasmon disperses is generally strongly affected at larger q by the reduced dimensionality of the GIC (implicit in $f(qd)$). Finally, the dispersion

coefficient scales at $\tilde{\beta}^2/\Omega_0$ and could, in principle be used to estimate β. The fundamental properties illustrated in this example are then:

(1) the plasma frequency provides a direct measurement of the shift of the Fermi energy, $k_F\beta$;

(2) the plasma frequency gives a somewhat cruder measure of the induced charge density ($\sim n^{1/4}$);

(3) the plasmon will disperse quadratically at small q;

(4) the dispersion coefficient probes the band dispersion parameter, β, and scales inversely as Ω_0.

We note that this simple model, while quite successful at identifying the relevant electronic parameters for these measurements, is inappropriate for a detailed quantitative analysis of the plasmon spectra. This latter analysis is sensitive to complications resulting from a non ideal band structure and local field effects in GIC's. Hence, in the following we resort to numerical analysis.

3. Band structure

We have constructed a nine parameter tight binding model to describe the graphite π electron band structure. These parameters describe interactions between elements of an orthonormal basis of π orbitals and include in plane interactions up to third nearest neighbors, interplane interactions up to second nearest neighbors on contiguous planes, a single interaction between nearest neighbors on second neighbor planes, and a slight shift in the diagonal matrix elements for the two distinct carbon sites (presumed to be of electrostatic origin [7] and relevant only for pristine graphite and stage III and higher stage compounds). The parameters were chosen to reproduce the 4.4 eV peak in $\epsilon_2(0, \omega)$ observed optically [8] while maintaining reasonably good agreement with the overall bandwidth and various gaps obtained in the LCAO analysis of Painter and Ellis [9] (which, in turn, is quite consistent with angle resolved photoemission data) [10]. We find remarkably little flexibility in the choice of these interaction parameters, which we conveniently derive by block diagonalizing the Hamiltonian at symmetry points and then fitting to a prescribed set of transition energies. The parameters are listed in Table 1 and the resulting band structure for 3D graphite is given in Fig. 1.

4. Evaluation of the longitudinal dielectric response function

Following the usual analysis of the self consistent response to an external perturbation of valence electrons in solid which interact *via* the coulomb interaction we obtain the dielectric response function [11, 12]

TABLE 1

Interaction parameters for π electrons in graphite
The notation $M^n_{\alpha\beta}$ denotes an interaction between orbitals on sites α and β on planes separated by n layers. Unprimed α, β denote nearest neighbor pairs between these layers, primed $\alpha\beta$ denote next neighbor pairs. Energies are in eV.

M^0_{aa}	= 0	
M^0_{bb}	= −0.1	
M^0_{ab}	= −2.63	
$M^0_{ab'}$	= −0.145	
$M^0_{aa'}$	= $M_{bb'}$ = 0.150	
M^1_{aa}	= −0.0875	
$M^1_{aa'}$	= 0.1042	
$M^1_{ab'}$	= −0.1563	M^2_{bb} = −0.0254
$M^1_{bb'}$	= −0.2333	

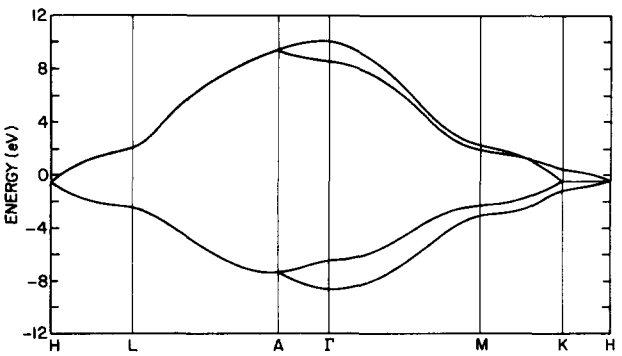

Fig. 1. Band structure of three dimensional graphite using the interaction matrix elements listed in Table 1.

$$\epsilon_{\vec{G},\vec{G}'}(\vec{q},\omega) = \epsilon_\infty \delta_{\vec{G},\vec{G}'} - \frac{4\pi e^2}{\Omega|\vec{q}+\vec{G}||\vec{q}+\vec{G}'|} \sum_{\vec{k},n,n'} \frac{[f_0(E_{n'}(\vec{k}+\vec{q})) - f_0(E_n(\vec{k}))]}{E_{n'}(\vec{k}+\vec{q}) - E_n(k) - \hbar\omega} \times \langle \vec{k},n|e^{i(\vec{q}+\vec{G})\cdot\vec{r}}|\vec{k}+\vec{q},n'\rangle\langle\vec{k}+\vec{q},n'|e^{-i(\vec{q}+\vec{G}')\cdot\vec{r}}|\vec{k},n\rangle \quad (6)$$

where ϵ_∞ is a background term, Ω is the unit cell volume, the f_0 are Fermi functions, the $\{\vec{G}\}$ are reciprocal lattice vectors and the sum extends over the Brillouin zone and band indices n and n'. The macroscopic (measured) dielectric function may then be recovered from eqn. (6):

$$\epsilon(q,\omega) = 1/\{\epsilon(q,\omega)\}^{-1}_{0,0}. \quad (7)$$

Dropping everything but the $G = G'$ terms in eqn. (6), expression (7) reduces to the Cohen–Ehrenreich dielectric function [13]. The off diagonal terms in eqn. (6) are very significant, however, since they incorporate microscopic

local field corrections into the dielectric function, which we anticipate to be very important whenever the eigenfunctions $|k, n\rangle$ in the solid differ significantly from plane waves. Thus, the off diagonal terms should be especially relevant in graphite, and even more so in GIC's, where π electron states are well localized to the individual graphite layers. To make the subsequent calculations, including local field effects, tractable we make the reasonable assumptions.

(1) that the eigenstates $|k, n\rangle$ may be factored into a product of a 2 dimensional Bloch function and a second function describing the localization of the basis functions to each layer graphite [14] and,

(2) that local field effects within the basal plane are insignificant so that we may drop $G \neq G'$ terms in eqn. (6) if $G-G'$ is not parallel to the c axis. With these assumptions, restricting our attention to q directed in the basal plane we reduce eqn. (6) to the form:

$$\epsilon_{\vec{G},\vec{G}'}(\vec{q}, \omega) = \epsilon_\infty \delta_{\vec{G},\vec{G}'} + \frac{\chi(\vec{q}, \omega)|q|^2}{|\vec{q} + \vec{G}||\vec{q} + \vec{G}'|} \rho^*(\vec{G})\rho(\vec{G}') \tag{8}$$

where $\chi(q, \omega)$ denotes a two dimensional "layer polarizability":

$$\chi(\vec{q}, \omega) = \frac{4\pi e^2}{\Omega |q|^2} \sum_{\vec{k},n,n'} \frac{\langle \varphi_{n,\vec{k}} | e^{i\vec{q}\cdot\vec{r}} | \varphi_{n',\vec{k}+\vec{q}} \rangle \langle \varphi_{n',\vec{k}+\vec{q}} | e^{-i\vec{q}\cdot\vec{r}} | \varphi_{n,\vec{k}} \rangle}{E_{n'}(\vec{k} + \vec{q}) - E_n(\vec{k}) - \hbar\omega}$$
$$\times [f_0(E_{n'}(\vec{k} + \vec{q})) - f_0(E_n/\vec{k}))] \tag{9}$$

where the φ are the two dimensional Bloch states suggested above and $\rho(G)$ are Fourier components of the c-axis profile of the charge density of each layer. The product form of the second expression in eqn. (8) allows an exact formal inversion of the dielectric matrix, from which we obtain the macroscopic dielectric function:

$$\epsilon(q, \omega) = \frac{\epsilon_\infty + \lambda_0 \chi(q, \omega)}{1 + \dfrac{\chi(q, \omega)}{\epsilon_\infty}(\lambda_0 - 1)} \tag{10}$$

where $\lambda_0 = \Sigma(|q|^2/|q + G|^2)\,|\rho(G)|^2$. If the c axis charge profile on each layer is given by a delta function, λ_0 may be evaluated exactly yielding [15]:

$$\lambda_0 = \frac{qd}{2} \frac{\sinh(qd)}{\cosh(qd) - 1}. \tag{11}$$

The plasmon frequencies are then given by the zeroes of the numerator of eqn. (10) [16]. ($f(q, d)$ of eqn. (1) = $4\pi\lambda_0/d$.) In general, however, λ_0 must be evaluated numerically, the profile $\rho(z)$ is taken as a Gaussian weighted by a polynomial with coefficients chosen to reproduce the position of the peak in the charge density of a Hartree–Fock–Slater C 2p orbital.

Finally, we comment on the evaluation of the matrix elements in eqn. (9). We may decompose $\varphi_{n,k}(r)$ into a set of Bloch orbitals:

$$\varphi_{n,k}(r) = \Sigma c^n_{kj} e^{ik.r} a_j(k, r). \tag{12}$$

Then each matrix element is expressable as an inner product on an operator $A(k, k+q)$:

$$\langle \varphi_n(k,r)|e^{-iq\cdot r}|\varphi_n'(k+q,r)\rangle = \Sigma c^n{}_{k,i}{}^* A_{ij}(k,k+q)c^{n'}_{k+q,j}. \tag{13}$$

The utility of expression (13) is that the A_{ij} are described quite accurately by a small q expansion. In fact $A_{ij} = \delta_{ij}$ holds for $|q| \sim$ half a Brillouin zone width. Thus the complete matrix element in eqn. (13), which is poorly approximated by a small q (dipole) expansion, may be accurately evaluated including higher multipole terms, merely be using the small q behavior of A, and the coefficients $\{c^n{}_k\}$ which are directly obtained in the band calculations.

Following evaluation of $\epsilon(q, \omega)$, the energy loss function Im $1/\epsilon(q, \omega)$ is obtained directly. Since the experiments under consideration are performed on HOPG samples in which macroscopic (micron diameter) microcrystals are aligned along the c axis but are randomly oriented in the basal plane, we average the energy loss cross section over an ensemble of basal plane orientations with respect to the direction of q. This has little effect on the plasmon peak position (which is reasonably isotropic with respect to rotations in the basal plane), but does smooth the shapes of the response functions $\epsilon_1(q, \omega)$ and $\epsilon_2(q, \omega)$ somewhat.

5. Results

In Fig. 2 we show two maps of electronic excitations in the q, ω plane for stage I and stage II $FeCl_3$ intercalated graphite, respectively. For the stage I calculations we assume a shift of the Fermi energy of 0.9 eV with

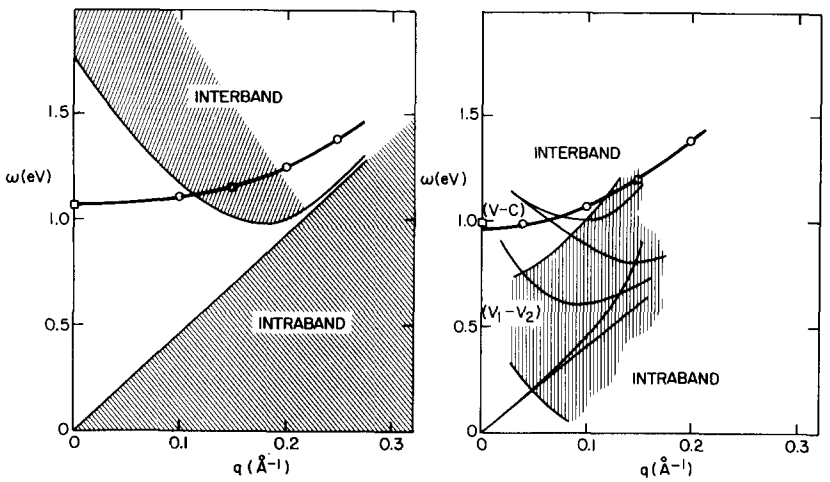

Fig. 2. Electronic excitation spectra in the q, ω plane in stage I (left) and stage II (right) $FeCl_3$ intercalated graphite. The heavy lines give the plasmon dispersion relation and the squares give the plasma frequencies measured in optical experiments.

respect to pristine graphite, and a background dielectric constant of 3. (We will comment on these fitted parameters later.) The effects of intercalation are to open a sizeable gap in the spectrum of single particle interband excitations and to introduce a strong, low frequency continuum due to intraband transitions. In response to these latter oscillators, ϵ_1 is driven sharply through zero, recrossing zero on the plasmon dispersion curve. The plasmon is weakly damped by the shaded interband continuum, but becomes increasingly strongly damped by a lifetime induced tail from the intraband spectrum as it approaches the continuum (for q approaching 0.25 Å^{-1}). The situation is considerably more complicated for the stage II compound as shown in the right hand panel. In this calculation a shift of the Fermi energy of 0.65 eV with respect to pure graphite is introduced, and again the background $\epsilon_\infty = 3$. As in the stage I compound, excitations within the band(s) which are partially depopulated by intercalation provide a very strong intraband continuum which extends down to $\omega = 0$. Somewhat weaker "intervalence" band transitions (*i.e.*, between the two lowest π bands) dominate the spectrum from 0.4 to 0.7 eV, and most of the valence conduction band excitations are located above 1 eV. The intervalence band excitations shown in this Figure, which are not present in the stage I material, are expected to have a rather pronounced effect on the plasmon, shown as the heavy solid line. In particular, we see that the plasmon crosses this intervalence threshold near $q = 0.12$ Å^{-1}, *i.e.*, long before it approaches the intraband threshold. Thus, these new stage II "intervalence" band excitations are expected rapidly to damp the plasmon as q increases.

These effects are illustrated in more detail in Fig. 3 where we compare the calculated and observed plasmon lineshapes in the two materials. An intrinsic electron lifetime of $\sim 1.8 \times 10^{-14}$ s (0.0375 eV) is included in these lineshape calculations. In the stage I material we see that the plasmon is a very well defined resonance at $q = 0.1$ Å^{-1}. Its intensity decays rapidly as q increases, though it is still a well defined excitation up to $q = 0.20$ Å^{-1}. Finally, in reasonable agreement with the experimental traces, the plasmon is severely overdamped as it closely approaches the intraband single particle continuum at $q = 0.25$ Å^{-1}. The stage II plasmon, on the other hand is considerably weaker at $q = 0.10$ Å^{-1} (note the vertical scale change) and is barely discernible past $q = 0.15$ Å^{-1} (as it crosses the intervalence threshold noted above), thus explaining the significantly more rapid decay observed experimentally.

In Fig. 4 we plot the theoretical and experimental dispersions obtained for the plasmons in stage I and stage II $FeCl_3$ intercalated graphite. In both the theoretical and experimental results for the two materials the dispersion is well described by a quadratic in q over the momentum range of interest. This is consistent with the discussion of Section 2, though that simple treatment would not justify the range in q over which the power law is observed to hold. The dispersion coefficients, which are expected to scale inversely as Ω_0 between the two systems, in fact change somewhat faster. This appears to be a bandstructure effect induced by antiscreening from the "inter-

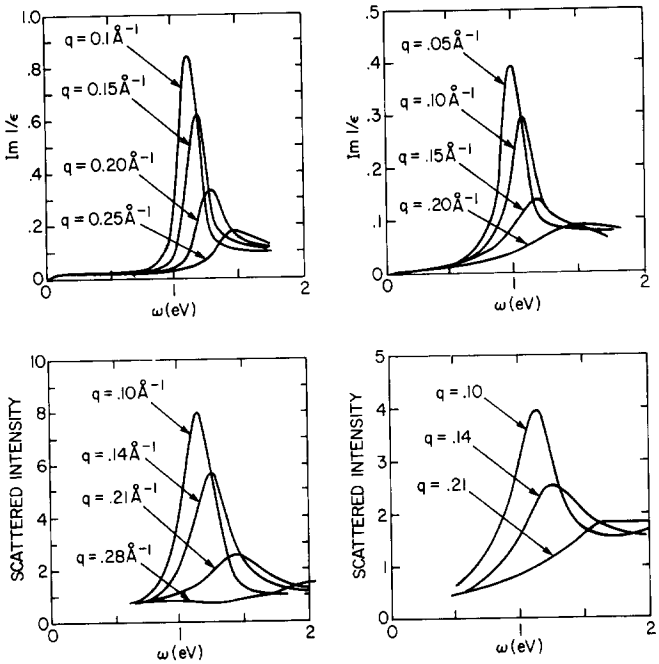

Fig. 3. Theoretical and experimental plasmon lineshapes for stage I (left) and stage II (right) $FeCl_3$ intercalated graphite. The theoretical results for the stage I and stage II compounds assume Fermi level shifts of 0.9 eV and 0.65 eV, respectively.

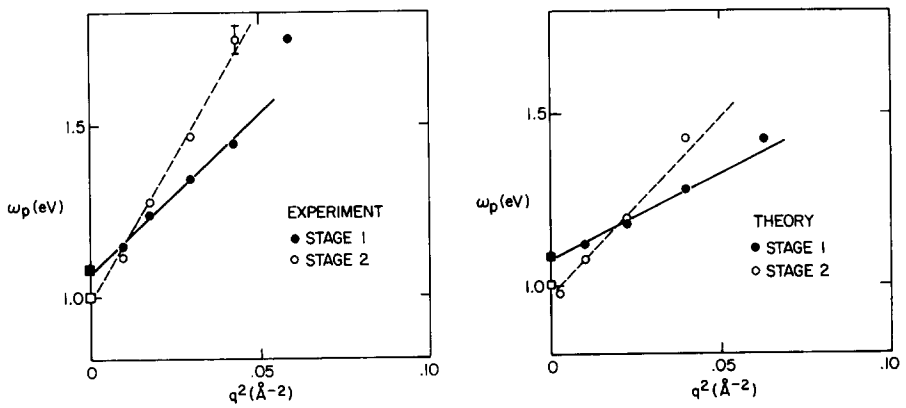

Fig. 4. Experimental and theoretical plasmon dispersion in stage I and stage II $FeCl_3$ intercalated graphite. The squares give plasma frequencies measured in optical experiments and the circles give measured or calculated results for inelastic electron scattering.

valence" oscillators below 1 eV in the stage II material. That is, the presence of intervalence oscillators above 0.4 eV in the stage II material displaces this plasmon to higher frequency than would be anticipated from the discussion of Section II.

Finally, the dispersion coefficients, given as the slopes of the theoretical results plotted in Fig. 4 fall systematically below the dispersion coefficients found experimentally. With reference to the results of Section 2 this is attributed to an underestimate of the band dispersion parameters in the model band structure. We note that previous calculations using a band structure with significantly larger dispersion (nearest neighbor interaction = 3 eV) provided a very satisfactory account of the plasmon dispersion [5], and it is quite likely that our current band parameters, which are chosen to provide overall agreement with theoretical and experimental data over the full Brillouin zone, may, in fact, provide a less accurate dispersion for these bands over a restricted region of the zone near the H–K axis. We conclude therefore that the experimental plasmon dispersion indicates that the π bands are slightly more dispersive near the H–K axis than is predicted in the model band structure.

In view of this uncertainty, it appears advisable to restrict attention to the momentum range $\leqslant 0.1$ Å^{-1} when fitting theoretical parameters to these experimental results. In this range the uncertainty in the plasmon dispersion has little effect on the calculated plasmon frequency which, we note, depends principally on the shift of the Fermi energy. For this reason, the Fermi energy shifts quoted above are obtained by fitting to experimental data at $q = 0.10$ Å^{-1}, *i.e.*, at the smallest momentum transfers experimentally accessible. Even with this precaution, these results may be affected slightly by the choice of background screening, $\epsilon_\infty = 3$ (which agrees very well with previous estimates from optical studies [17]). Further variation of ϵ_∞ in the range $2 < \epsilon_\infty < 4$ introduces ± 50 meV shifts in the calculated plasmon peak positions. Short of a far more detailed microscopic theory there seems to be no unambiguous method for excluding ϵ_∞ values somewhat higher or assessing the stage dependence of this quantity. For the present, we note that the background screening chosen in these calculations is quite plausible and the results are reasonably insensitive to small variations in this value.

Integrating our model densities of states over the Fermi energy shift fitted in these calculations we estimate a conduction charge density of ~ 0.027 holes/C in the stage I compound and ~ 0.014 holes/C in the stage II compound. Despite the possible absolute errors in these estimates enumerated above, it is quite interesting that the stage II value is quite accurately given as half the value of the stage I charge transfer. This result, and the fitted Fermi level positions, are in quite good agreement with Fermi level positions identified from analysis of the C 1s core exciton lineshape in these compounds [4].

6. Conclusion

We have presented a theoretical analysis of the low frequency plasmon spectra in stages I and II $FeCl_3$ intercalated graphite. Many of the differences

between the plasmon spectra in these two compounds are anticipated and qualitatively explained on the basis of a simple model for the dielectric response functions. The real systems, however, are sufficiently non-ideal, to be quantitatively sensitive to band structure effects (and, to a lesser extent, local field effects) in these solids. Numerical calculations including these effects provide a good description of the observed spectra. Fitting theoretical spectra to experimental data at $q = 0.10$ Å^{-1} we estimate Fermi energy shifts of 0.9 eV and 0.65 eV in stages I and II $FeCl_3$ intercalated graphite, respectively, with respect to pristine graphite.

References

1 J. J. Ritsko and M. J. Rice, *Phys. Rev. Lett., 42* (1979) 666; J. J. Ritsko and E. J. Mele, *Phys. Rev. B, 21* (1980) 730.
2 D. M. Hwang, M. Utlaut, M. S. Isaacson and S. A. Solin, *Phys. Rev. Lett., 43* (1979) 882.
3 E. J. Mele and J. J. Ritsko, *Phys. Rev. Lett., 43* (1979) 68.
4 J. J. Ritsko and E. J. Mele, *Physica, 99B* (1980) 425.
5 E. J. Mele and J. J. Ritsko, *Solid State Commun., 33* (1980) 937.
6 Similar conclusions are reached in analysis of optical spectra by J. Blinowski, N. H. Hau, C. Rigaux, J. Vieren, R. LeToullec, G. Furdir, A. Hérald and J. Melin, *J. Phys. (Paris), 41* (1980) 47.
7 J. W. McClure, *Phys. Rev., 108* (1957) 612. Several empirical band structure models exist, *e.g.*, M. S. Dresselhaus, G. Dresselhaus and J. E. Fischer, *Phys. Rev. B, 15* (1977) 3180 or N.A.W. Holzwarth, *Phys. Rev. B*, in press.
8 E. A. Taft and H. R. Phillip, *Phys. Rev., 137* (1965) A197.
9 G. S. Painter and D. E. Ellis, *Phys. Rev. B, 1* (1970) 4747.
10 W. Eberhardt, I. T. McGovern, E. W. Plummer and J. E. Fischer, *Phys. Rev. Lett., 44* (1980) 200.
11 S. L. Adler, *Phys. Rev., 126* (1962) 413.
12 N. Wiser, *Phys. Rev., 129* (1963) 621.
13 H. Ehrenreich and M. H. Cohen, *Phys. Rev., 115* (1959) 786.
14 This may be rigorously justified if either (a) the two dimensional eigenstates are plane waves or (b) if the π electron basis functions are Gaussian.
15 This approach is similar to the treatment of umklapp processes in quasi one dimensional systems given by P. F. Williams and A. N. Bloch, *Phys. Rev. B, 10* (1974) 1097.
16 Here we recover the form of the dielectric function derived in ref. 5. Similar analysis for a two dimensional system ($d \to \infty$) is given by F. Stern, *Phys. Rev. Lett., 18* (1967) 5461.
17 L. G. Johnson and G. Dresselhaus, *Phys. Rev. B, 7* (1973) 2275. In this paper ϵ_∞ = 2.5.